JACS
JOURNAL OF THE AMERICAN CHEMICAL SOCIETY

Article

pubs.acs.org/JACS

Dipole-Moment-Driven Cooperative Supramolecular Polymerization

Chidambar Kulkarni,[†,§] Karteek K. Bejagam,[§] Satyaprasad P. Senanayak,[§] K. S. Narayan,[§] S. Balasubramanian,*[,§] and Subi J. George*[,†]

[†]New Chemistry Unit, Jawaharlal Nehru Centre for Advanced Scientific Research, Jakkur, Bangalore 560064, India

[§]Chemistry and Physics of Materials Unit, Jawaharlal Nehru Centre for Advanced Scientific Research, Jakkur, Bangalore 560064, India

Supporting Information

ABSTRACT: While the mechanism of self-assembly of π-conjugated molecules has been well studied to gain control over the structure and functionality of supramolecular polymers, the intermolecular interactions underpinning it are poorly understood. Here, we study the mechanism of self-assembly of perylene bisimide derivatives possessing dipolar carbonate groups as linkers. It was observed that the combination of carbonate linkers and cholesterol/dihydrocholesterol self-assembling moieties led to a cooperative mechanism of self-assembly. Atomistic molecular dynamics simulations of an assembly in explicit solvent strongly suggest that the dipole−dipole interaction between the carbonate groups imparts a macro-dipolar character to the assembly. This is confirmed experimentally through the observation of a significant polarization in the bulk phase for molecules following a cooperative mechanism. The cooperativity is attributed to the presence of dipole−dipole interaction in the assembly. Thus, anisotropic long-range intermolecular interactions such as dipole−dipole interaction can serve as a way to obtain cooperative self-assembly and aid in rationalizing and predicting the mechanisms in various synthetic supramolecular polymers.

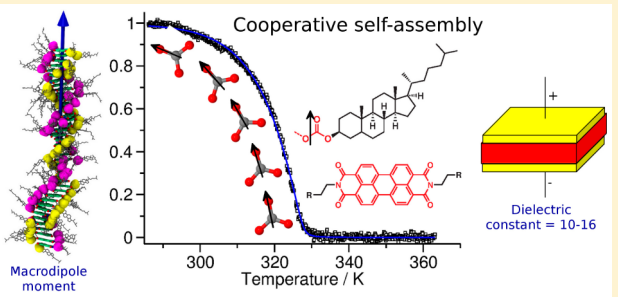

INTRODUCTION

Synthetic macromolecules assembled from monomers capable of exhibiting intermolecular interactions such as hydrogen-bonding, π-stacking, amphiphilic, and electrostatic interactions have been studied to mimic their biological counterparts and for materials applications.[1−6] The investigation into the mechanism of supramolecular polymerization has gained importance in the past decade to allow for a better control over its structure and functions.[7−13] The mechanism of non-covalent one-dimensional (1-D) polymerization has been broadly classified into two types: isodesmic and cooperative.[14] A cooperative or nucleation−elongation mechanism has been observed in biopolymers such as actin[15] and flagellin.[16] Thermodynamic aspects of self-assembly and their relationship with mechanism have been studied extensively.[14,17,18] In their seminal review, Meijer and co-workers suggested electronic, structural, and hydrophobic interactions as the cause of cooperativity in supramolecular polymers.[14] Hitherto, a comprehensive rationale for the observed mechanisms of polymerization based on structural motifs in the monomer is lacking.

Benzene-1,3,5-tricarboxamide[19−21] derivatives are seminal examples of cooperative supramolecular polymerization involving intermolecular hydrogen-bonding in the stacking direction. In addition, many π-conjugated systems studied in the literature that are likewise capable of intermolecular hydrogen bonding have also been shown to follow the cooperative mechanism of self-assembly.[22−28] However, there are a few exceptions where the system apparently lacks hydrogen bonding along the stacking direction and yet shows a cooperative mechanism of self-assembly.[29,30] Recently, cooperativity has also been observed in π-conjugated systems with a variety of other intermolecular interactions operating in the growth direction.[31−34] In order to rationalize the observed mechanisms in a broader sense, we had previously proposed the necessity of anisotropic long-range interactions between monomers (or small stacks) for a cooperative self-assembly.[35] Dipolar interaction is one such, and it has also been used to construct supramolecular polymers.[36] The effect of dipolar groups present in a molecule on the mechanism of supramolecular polymerization has seldom been studied. Recently, Würthner and co-workers have shown the cooperative supramolecular polymerization of dipolar merocyanine dyes.[37]

Perylene-3,4,9,10-tetracarboxylic acid bisimides (PBIs) are well-known electron-deficient organic semiconductors and have been widely employed as active materials in organic electronics.[38,39] PBI derivatives are known to follow an isodesmic mechanism of self-assembly.[40−43] However, there are only a few reports (by the groups of Würthner, Meijer, and Yagai) on the cooperative self-assembly of PBIs; these are mainly driven by either intermolecular hydrogen bonding or intramolecular hydrogen bonding together with π-stacking.[44−47]

Received: January 16, 2015

DOI: 10.1021/jacs.5b00504
J. Am. Chem. Soc. XXXX, XXX, XXX−XXX

In the present study, we investigate the effect of dipolar groups and different self-assembling moieties appended to PBI on the mechanism of self-assembly. Here we observe cooperative self-assembly of PBI derivatives containing no apparent hydrogen-bonding groups. Extensive spectroscopy, molecular dynamics (MD) simulations, and bulk dielectric measurements were performed on these molecules to shed light on the origin of cooperativity. Herein, we show that dipole−dipole interaction between monomers along the stacking direction is the primary cause of cooperativity. The interaction is shown to arise from the dipolar nature of carbonate linkers and the rigidity of cholesterol self-assembling moieties. Thus, we present a unique example of non-hydrogen-bonded and dipole-moment-driven cooperativity in a supramolecular system.

RESULTS

The molecular design involves utilizing the optical properties of the PBI core to probe the mechanism of self-assembly by varying the linker group (either carbonate or ether) and self-assembling moiety (cholesterol or alkyl groups, Figure 1).

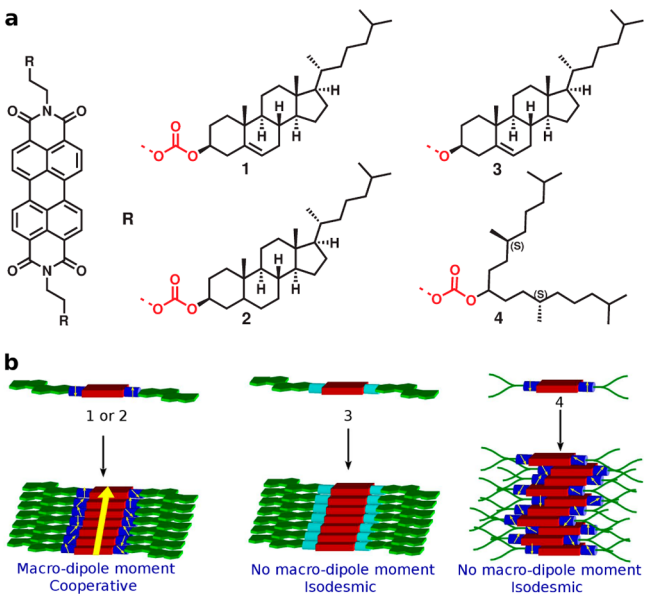

Figure 1. Molecules under study. (a) PBI is functionalized on both imide nitrogens with either carbonate or ether linker (marked in red). Cholesterol (**1** and **3**), dihydrocholesterol (**2**), and chiral swallowtail (**4**) are used as the self-assembling motifs. (b) Schematic representation of the assembly of different PBI derivatives. PBIs are depicted by red blocks. Blue and cyan cylinders represent carbonate and ether linkers, respectively. Self-assembling moieties are shown in green. Small yellow arrows indicate molecular dipoles along the carbonate C═O axis. Macro-dipole moment is shown as a large yellow arrow along the stacking direction.

Dialkyl carbonates are known to possess dipole moment in different conformations[48] and are thus utilized as the source of molecular dipole moment. An ethylene spacer is chosen to be placed between the imide nitrogen and the carbonate to provide appropriate solubility and rigidity to the molecule. **1** and **2** contain dipolar linkers (carbonate) and a rigid steroid-based self-assembling moiety. In contrast, **3**, possessing ether linkers, differs only in the absence of dipolar groups, thus allowing us to study the effect of linkers on the mechanism of self-assembly. In **4**, the steroid moiety of **1** is exchanged for a chiral swallowtail, so as to be able to examine the effect of this moiety on the mechanism of self-assembly. Synthesis of molecules **1**−**4** was carried out by coupling of the corresponding chloroformates[49] with *N*-Boc-ethanolamine, followed by deprotection to yield the respective amines. Condensation of the respective amines with perylene-3,4,9,10-tetracarboxylic acid dianhydride yielded the target molecules. All molecules were characterized by ^{1}H and ^{13}C NMR, IR, and mass spectroscopy (see Supporting Information (SI) for experimental details and characterization).

Self-Assembly Studies. UV/vis absorption spectrum of **1** in chloroform ($c = 1 \times 10^{-5}$ M) shows prominent peaks at 525 ($\varepsilon = 74\,200$ M^{-1} cm^{-1}), 488, 458, and 260 nm. The absorption features between 450 and 530 nm have been attributed to the vibronic bands of $S_0 \rightarrow S_1$ transition of PBIs along the long axis of the molecule.[50] The corresponding fluorescence spectrum shows a mirror image of the absorption spectrum with a maximum at 538 nm (SI, Figure S6a,b). These absorption and fluorescence spectral features are characteristic of $\pi-\pi^*$ transitions of PBIs devoid of intermolecular interactions.[39] The UV/vis absorption spectrum of **1** in methylcyclohexane (MCH) shows the loss of vibronic features, with an absorption maximum at 473 nm and a broad band centered around 555 nm. The fluorescence spectrum of **1** in MCH shows the quenching of monomer emission (at 538 nm by 39 times) and the emergence of a new band at 640 nm (inset of SI, Figure S6b). The fluorescence excitation spectrum of **1** in MCH obtained by monitoring the emission intensity at 565 and 650 nm shows well-resolved vibronic bands (400−550 nm) and a broad band centered around 470 nm, respectively (see SI, Figure S7). These spectral features indicate that the fluorescence of **1** at 565 nm is due to the residual monomers and that at 650 nm arises from the aggregates. The hypsochromic shift of the absorption maximum and quenching of monomer emission points to the face to face H-type of aggregate formation of **1** in MCH.[42] Similar H-type aggregate formation has been observed for **2** (Figure S8), **3** (Figures S9 and S10) and **4** (Figure S11) in apolar solvents like MCH (see SI). Nanostructures of aggregates of **1**−**4** have been characterized through dynamic light scattering studies and atomic force microscopy. These studies reveal 1-D aggregation of molecules **1**, **2**, and **4** (see SI, Figures S12−S15, for details). On the other hand, **3** forms spherical particles. It has been observed earlier that some of the bischolesterol derivatives self-assemble into 1-D structures, and further higher order aggregation leads to formation of spherical particles.[51]

The cholesterol moiety possessing chiral centers has been utilized for the organization of various chromophores.[52−54] It has an additional role in acting as a source of chiral bias to organize the π-conjugated molecules into helical assemblies by imparting van der Waals interaction to stabilize the assemblies.[55] Circular dichroism (CD) spectra of **1** in MCH and 1,1,2,2- tetrachloroethane (TCE) (95:5, v/v) ($c = 1 \times 10^{-5}$ M) showed a bisignated positive Cotton effect with positive and negative maximum at 485 and 450 nm, respectively (Figure 2a), suggesting the right handed chiral organization of the PBI core due to the presence of cholesterol moiety.[56] Further, by heating the solution, CD effect (mdeg) decreased in magnitude, and beyond 70 °C it vanishes (Figure 2a), suggesting the loss of chiral organization of the assembly. The corresponding temperature-dependent UV/vis absorption spectra show the evolution of vibronic features (characteristic of monomers) with an increase in temperature (Figure 2b). This observation

DOI: 10.1021/jacs.5b00504
J. Am. Chem. Soc. XXXX, XXX, XXX−XXX

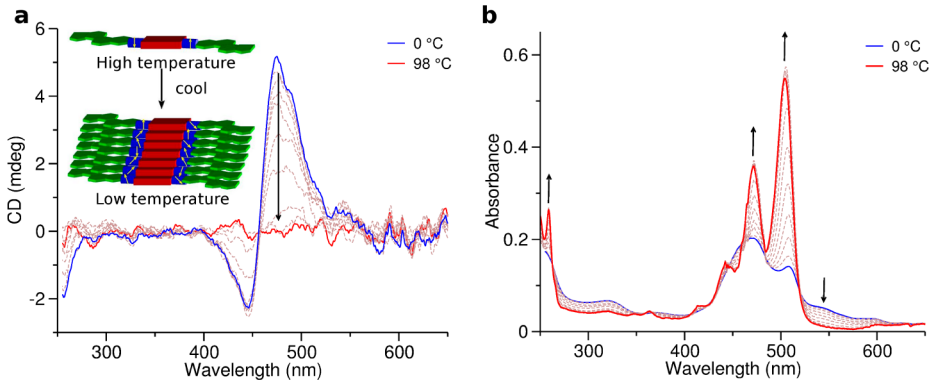

Figure 2. Self-assembly of **1**. Temperature-dependent CD (a) and UV/vis absorption spectra (b) of **1** in MCH/TCE (95:5, v/v) at every 10 °C. All studies were done at a concentration of 1×10^{-5} M in a 10 mm cuvette. Inset of (a) shows a schematic representation of the assembly at high and low temperatures. Arrows indicate spectral changes with an increase in temperature.

indicates that the CD spectral changes (with temperature) are indeed due to the disassembly of the aggregates. CD spectra of dihydrocholesterol appended derivative with carbonate linker (**2**) (Figure 3 and SI, Figure S16) and cholesterol tethered

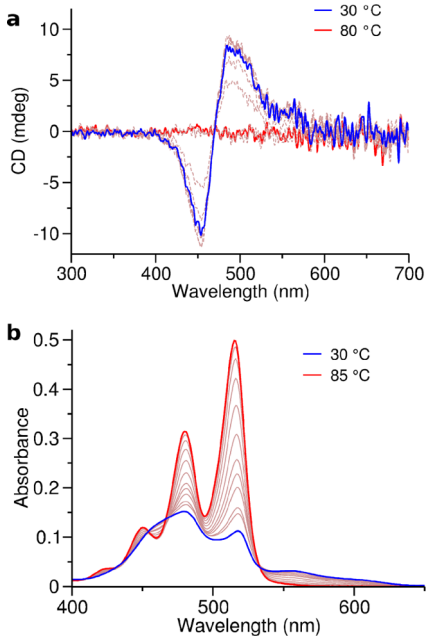

Figure 3. Self-assembly of **2**. Temperature-dependent CD (a) and UV/vis absorption spectra (b) of **2** ($c = 8 \times 10^{-6}$ M) in MCH/TCE (95:5, v/v).

derivative (**3**) (SI, Figure S17) in the self-assembled state show positive and negative Cotton effect, respectively, indicating a chiral supramolecular organization. The sign and magnitude of the CD spectra vary with aging and cooling rate,[57] as observed in other cholesterol- and dihydrocholesterol-based gelators,[54,58] probably due to the presence of multiple stereocenters (which compete among themselves) in the self-assembling moiety. Molecule **3** also exhibited a bisignated Cotton effect, suggesting the chiral organization of molecules in the assembly (SI, Figure S17). On the other hand, carbonate linker possessing **4** was CD silent (SI, Figure S18), probably due to the high flexibility of the chiral swallowtails, which hinders any chiral organization in the assemblies (*vide infra*, MD simulations).

Mechanism of Self-Assembly. The temperature dependence of the degree of aggregation (α) has been employed in the literature to ascertain the mechanism of self-assembly.[26,29,59] Utilizing the same methodology, we study the self-assembly mechanism of **1**–**4** by monitoring changes in either CD or UV/vis absorption spectra at a particular wavelength (characteristic of the assemblies) as a function of temperature. The normalized change in CD monitored at 480 nm for a solution of **1** (carbonate linker and cholesterol motif) as a function of temperature (cooling curve) is clearly non-sigmoidal (Figure 4a).

The experimental data are in agreement with the fit obtained by the Eikelder–Markvoort–Meijer (EMM) model for a nucleation–elongation mechanism for a one-component system,[60,61] indicating a cooperative (or nucleation–elongation) mechanism of self-assembly of **1**. The temperature in the cooling curve at which the self-assembly begins is termed as elongation temperature (T_e). The relevant thermodynamic parameters for the self-assembly of **1** at various concentrations have been obtained from the fitting of the cooling curves (SI, Table S2). In addition, temperature-dependent UV/vis studies also exhibited a critical point in the cooling curve (SI, Figure S21 and Table S3), reaffirming the cooperative nature of the self-assembly of **1**. It is observed that as the total concentration of the solution increases, T_e increases, while other thermodynamic parameters like ΔG^0 and cooperativity factor are nearly identical. Similar effects of concentration on T_e have been reported in literature for other systems.[19]

Dihydrocholesterol- and cholestero-based ALS (where A = aromatic, L = linker, and S = steroidal groups) systems have been shown to differ significantly in their gelation properties.[62] Since dihydrocholesterol is a rarely used self-assembling motif, it is interesting to note its effect on the mechanism of self-assembly. Thus, the cooling curves obtained for **2** (carbonate linker and dihydrocholesterol motif) by monitoring changes in CD spectra (Figure 3a) and UV/vis absorption spectra (Figure 3b) at different concentrations also showed a non-sigmoidal behavior (Figure 4b and SI, Figures S24 and S25); the experimental data are well described by the nucleation–elongation model. Cooling curves monitored at two different wavelengths (475 and 560 nm) show similar T_e, indicating that both absorption bands correspond to the same aggregate (SI, Figure S27).

Apart from temperature, concentration can also be used to vary the extent of aggregation, and such concentration-

DOI: 10.1021/jacs.5b00504
J. Am. Chem. Soc. XXXX, XXX, XXX–XXX

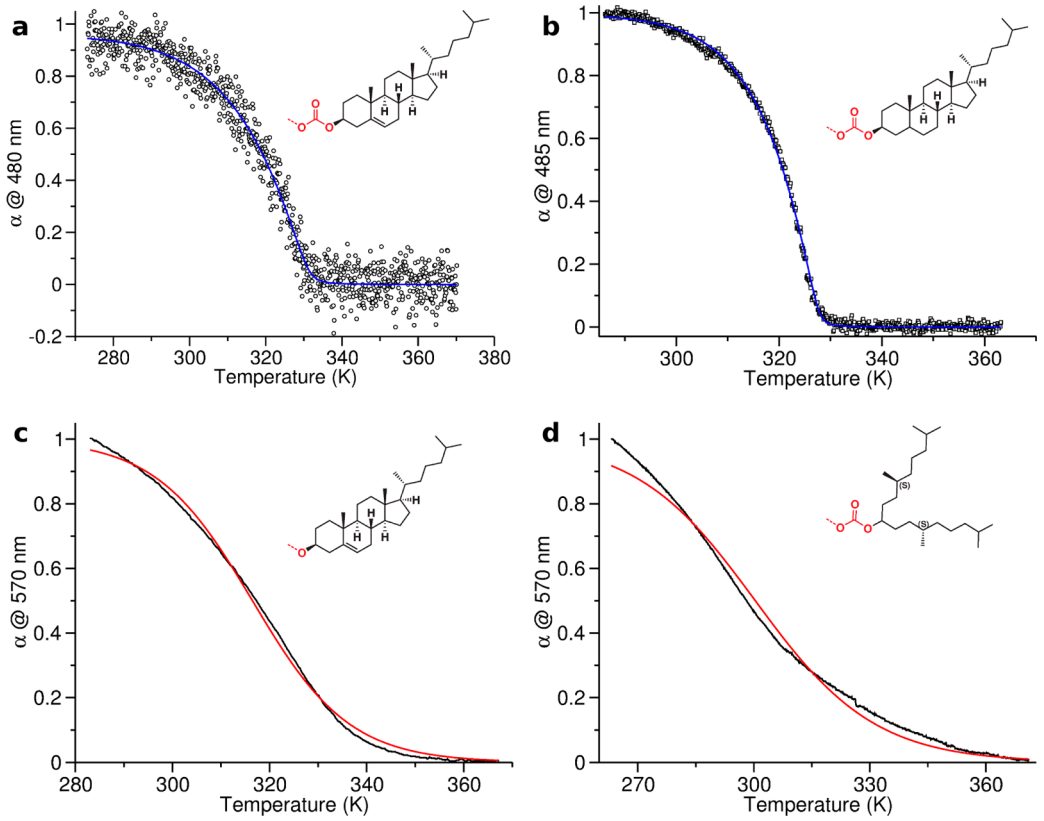

Figure 4. Mechanism of self-assembly of **1**–**4**. (a,b) Degree of aggregation (α) as a function of temperature (cooling curve) for a solution (95% MCH and 5% TCE) of **1** and **2**, respectively, by monitoring the CD effect at 480 nm (for **1**) and 485 nm (for **2**) at a cooling rate of 2 K/min (c = 8.0 × 10^{-6} M). (c) Cooling curve obtained by monitoring changes in UV/vis absorbance of **3** at 570 nm at a cooling rate of 1 K/min (c = 2 × 10^{-5} M in 80% MCH and 20% TCE). (d) Normalized change in UV/vis absorbance of **4** as a function of temperature, monitoring the absorbance at 570 nm (cooling rate 2 K/min, c = 4.69 × 10^{-4} M, in MCH). The solid blue and red lines are the fits obtained from nucleation–elongation and isodesmic models, respectively. The structures of linker and self-assembling group corresponding to each of the molecules are shown as insets.

dependent studies have been extensively used by Würthner and co-workers to ascertain the mechanism of self-assembly.[37,42] Thus, concentration-dependent UV/vis absorption studies of **2** in MCH/TCE (95:5, v/v) were performed. The transition from monomers to aggregates occurs within a narrow concentration range of 2.5 × 10^{-6}–3.3 × 10^{-6} M (SI, Figure S28), thus indicating the cooperative mechanism of self-assembly.

Interestingly, the cooperativity parameter (σ, obtained from fitting the experimental cooling curve to the EMM model[60,61]) for **2** was found to be consistently (by both CD and UV/vis measurements) lower than that for **1** (Table 1), suggesting a higher degree of cooperativity in the former system compared to that in the latter. σ is of the order of 10^{-3} for **1**, whereas for systems containing intermolecular hydrogen bonds, it is found in the range of 10^{-3}–10^{-6}.[19,22−28] Despite the lack of any apparent hydrogen-bonding motif, the present systems (**1** and **2**) show cooperativity comparable to conventional hydrogen-bonded systems. In addition, **2** shows: a lower cooperativity factor σ, more negative ΔG^0, and lower solubility compared to **1** (Table 1). These differences can be mainly attributed to the structural planarity of dihydrocholesterol compared to cholesterol, which enhances van der Waals interaction between the moieties in an assembly.[62]

Table 1. Comparison of Thermodynamic Parameters for the Assembly of 1 and 2 (in 95% MCH and 5% TCE)

molecule	ΔH_e (kJ/mol)	ΔS_e (kJ/mol)	ΔG^0 (kJ/mol)	cooperativity factor, σ
1	−41.61	−0.027	−33.45	2.4 × 10^{-3}
2	−89.98	−0.17	−37.25	2.0 × 10^{-4}

Values presented are average of those obtained by fitting to the EMM model[60,61] for **1** and **2** (from CD and UV/vis studies at different concentrations). The values for **1** are averages of those presented in SI, Tables S2 and S3. ΔG^0 was calculated at 298.15 K.

The self-assembly mechanisms of **3** (ether linker and cholesterol motif) and **4** (carbonate linker and chiral swallowtail) were also studied using temperature-dependent UV/vis spectroscopy.[63] A solution (c = 2 × 10^{-5} M in MCH/TCE (8:2, v/v)) of **3** showed the gradual evolution of the extent of aggregation with decrease in temperature (Figure 4c). The cooling curve could well be described by the isodesmic model,[59] yielding an enthalpy of polymerization (ΔH) of −92.0 kJ mol^{-1} and melting temperature (T_m, temperature at which α = 0.50) of 316.5 K. Similarly, the cooling curve for **4** (in MCH, c = 4.69 × 10^{-4} M) showed a sigmoidal behavior and could be fit to an isodesmic model (Figure 4d),[64] yielding the thermodynamic parameters ΔH = −53.5 kJ mol^{-1} and T_m = 300.4 K. Thus, the linker group of the monomer significantly affects the mechanism of self-assembly.

Since **4** is isodesmic and weakly aggregating, another derivative of PBI (**PBI_carb_dd**) possessing linear dodecyl chains in place of branched chains (**4**) was synthesized to investigate its effect on the mechanism of self-assembly. **PBI_carb_dd** self-assembles into J-aggregates (SI, Figure

DOI: 10.1021/jacs.5b00504
J. Am. Chem. Soc. XXXX, XXX, XXX−XXX

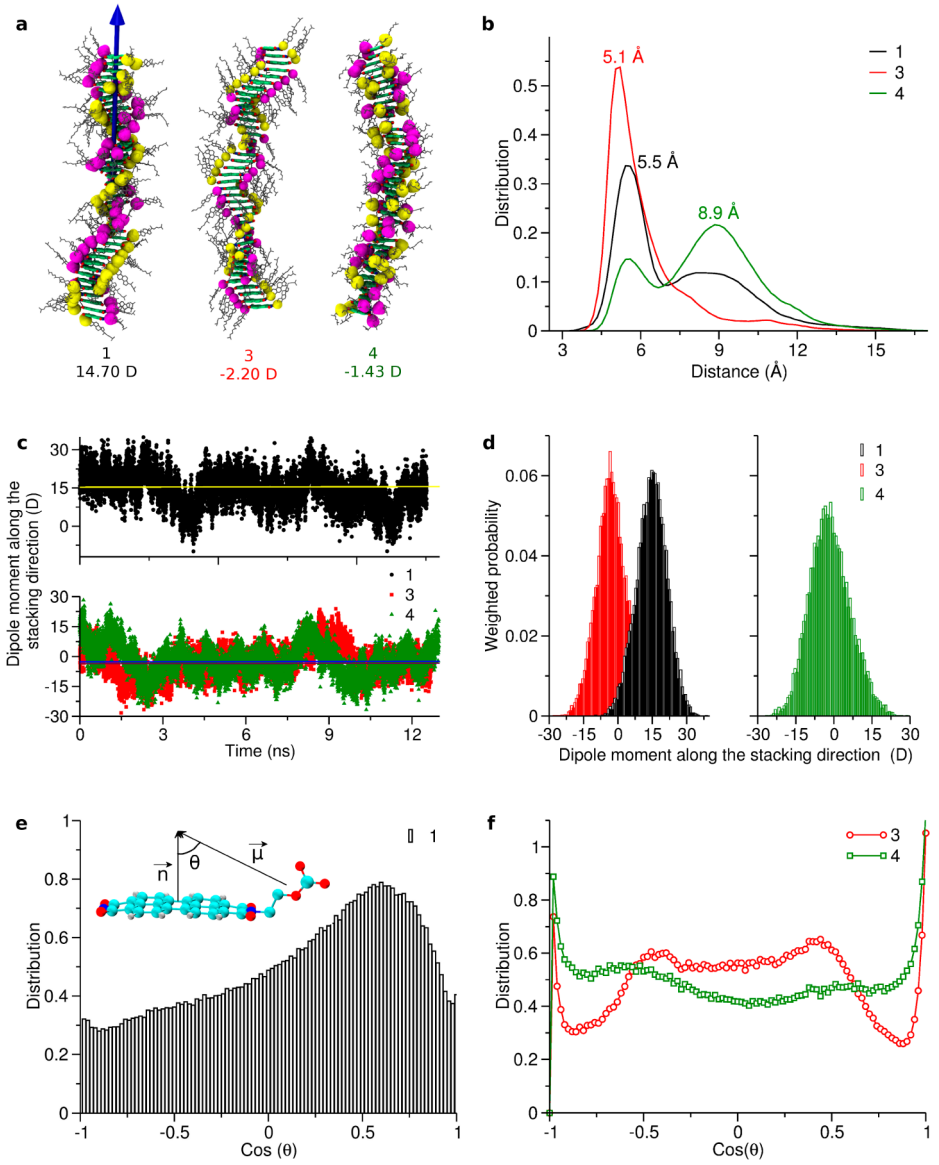

Figure 5. MD simulations of the assemblies of **1**, **3**, and **4**. (a) Snapshot illustrating the arrangement of molecules in the assembled state. Linkers are highlighted in yellow and magenta to aid in the visualization of the helical packing. Self-assembling groups are represented with thin sticks, and hydrogens are omitted for clarity. (b) Distance distribution between the linkers of neighboring molecules. (c) Macro-dipole along the stacking direction as a function of time. Solid horizontal lines (yellow for **1**, blue for **3**, and maroon for **4**) are drawn to represent the mean dipole moment value for each system. (d) Weighted probability distribution of macro-dipole obtained from (c). (e,f) Distribution of the cosine of the angle between the dipole moment of each molecule ($\boldsymbol{\mu}$) with the normal to the PBI plane (**n**). All the analysis was performed on the last 12 ns of the MD trajectory.

S32) and exhibits a cooperative mechanism of self-assembly (SI, Figure S33).

Molecular Dynamics Simulations. Computational studies were undertaken to gain further insight into the molecular organization of the assemblies and to elucidate the role of different moieties on the self-assembly mechanism. Quantum chemical calculations are computationally expensive in determining the equilibrium structure of assemblies due to the large number of atoms. On the other hand, MD simulations can describe the molecular packing in these supramolecular assemblies.[65−70] In particular, MD simulations are well suited to treat the effect of solvents and temperature, so as to realize experimental conditions. Thus, MD simulations were carried out to investigate the molecular packing in the aggregated state for **1**, **3**, and **4** and to understand the mechanism of their self-assembly in terms of intermolecular interactions. Simulations of pre-formed oligomeric stacks, each containing 40 molecules of **1**, **3**, and **4** were performed in explicit cyclohexane at 298.15 K for 20 ns (see SI, Figures S35−S37 and Tables S4 and S5, for more details).[71]

Snapshots at the end of the MD simulations for cholesterol appended molecules **1** and **3** exhibit helical packing of linker groups (carbonate or ether) around the PBI core (Figure 5a). This, in turn, is reflected in the ordered helical organization of the peripheral cholesterol groups and PBI core, in agreement with the experimental observation of bisignated CD signal (Figure 2). On the other hand, the organization of linker groups (carbonate) in the assembly of **4** is ill-defined (Figure 5a) which can be attributed to the flexibility of the chiral swallowtail. Coincidentally, chiral organization in **4** is experimentally determined to be absent as well (SI, Figure S18). The arrangement of linkers in the assembly can be further

DOI: 10.1021/jacs.5b00504
J. Am. Chem. Soc. XXXX, XXX, XXX−XXX

quantified by the distance between them across neighboring molecules in an assembly (Figure 5b). Assemblies of **1** and **4** exhibit a bimodal distribution of interlinker (carbonate) distances, centered at 5.5 and 9 Å. For **1**, the intensity at 5.5 Å is larger than at 8.9 Å, suggesting that the majority of carbonate groups are more closely arranged in an assembly of **1** compared to that of **4**. A unimodal probability distribution centered at 5.1 Å is observed for the assembly of **3** (ether linker), suggesting close and uniform packing of linkers. (For further discussion see section "Origin of the bimodal distribution of the linker distances" in SI and Figures S42 and S43.) The inclination angle of the carbonate vector, in two helices, with respect to the normal of PBI plane is shown in SI, Figure S40. The average of this quantity can be taken as an order parameter for structural ordering. This quantity averaged over the core 30 molecules for **1** and **4** is 0.149 and 0.005, respectively, clearly suggesting the ordered arrangement of molecules in the former over the latter. Thus, the differences in the structural organization can be attributed to the rigidity or flexibility of the self-assembling moiety.

The consequence of structural organization of linkers on the macro-dipole moment (along the stacking direction) is studied during the MD trajectory (Figure 5c,d). Macro-dipole is calculated as $\sum q_i \mathbf{r}_i$, where q_i is the charge on the atoms and $\mathbf{r}_i$ the displacement vector from negative to positive charge, respectively, and the sum extends over all atoms. The mean macro-dipole moment for **1** (14.7 D) is an order of magnitude higher than that for **4** (1.43 D), although in both molecules (**1** and **4**), the carbonate linker is the dipolar entity. We now study the orientation of the dipole moment of a molecule. In order to eliminate edge effects, we discard contributions from five molecules present at either end of the stack in further analysis. The distribution of the angle between the dipole moment vector ($\boldsymbol{\mu}$) of each molecule with the normal of its PBI plane ($\mathbf{n}$) is shown in Figure 5e,f. For **3** and **4**, the distribution is nearly symmetric about zero (Figure 5f), implying that parallel and antiparallel orientations of molecular dipoles are equally likely which does not lead to any significant macro-dipole for the stack. In contrast, in the assembly of **1**, the carbonate linkers on each branch of the molecules are better aligned with each other; however, the net dipole from each of these branches, although in opposite directions, do not cancel fully. This results in a net macro-dipole moment for a stack of **1** (details in SI). Thus, the difference in the macro-dipole moment between **1** and **4** can be mainly attributed to the organization of the linkers.

Dielectric Measurements. A significant macro-dipole moment in **1** and none in **4** would be reflected in the dielectric constants of these molecules. Capacitance measurement is a direct experimental means of quantifying the extent of polarization in the system. Thus, we have measured the bulk (thin-film state) capacitance for assemblies of **1**−**4** to evaluate the magnitude of polarization and to correlate with the mechanism of self-assembly at the molecular level.

The dielectric constant, $\varepsilon_r = Cd/\varepsilon_0 A$ (where C is capacitance, d film thickness, ε_0 vacuum permittivity, and A area of the film obtained from the capacitive response), is essentially a measure of the macroscopic dipole moment.[72] Molecules **1** and **2**, which exhibit a cooperative self-assembly, display higher polarization indicated by the higher magnitude of ε_r (Figure 6a). It should be noted that this magnitude of ε_r ($\approx$ 16 for molecule **2**) is around 5 times higher than the ε_r observed for molecules **3** and **4**, which do not follow a cooperative mechanism of self-assembly. Classical theory of linear dielectrics based on Clausius−Mossotti relation is used to estimate the polarizability at zero frequency of the molecules.[73] The effective dipole moment per molecule ($|\boldsymbol{\mu}|$) estimated from the dielectric constant measurement of the assembly was in the range of 3−5 D for molecules **1** and **2**. In comparison, the $|\boldsymbol{\mu}|$ values for molecules **3** and **4** were in the range of 0.6−0.7 D. The value of $|\boldsymbol{\mu}|$ for molecules **1**, **3**, and **4** estimated from MD simulation is 10 times lower than the experimentally obtained value.[74] This can be attributed to the difference in the measurement conditions (such as condensed phase) versus that in the simulations which were carried out in the solution phase. However, the trends in dipole-moment values are same across different molecules obtained from both MD simulations and dielectric measurements.

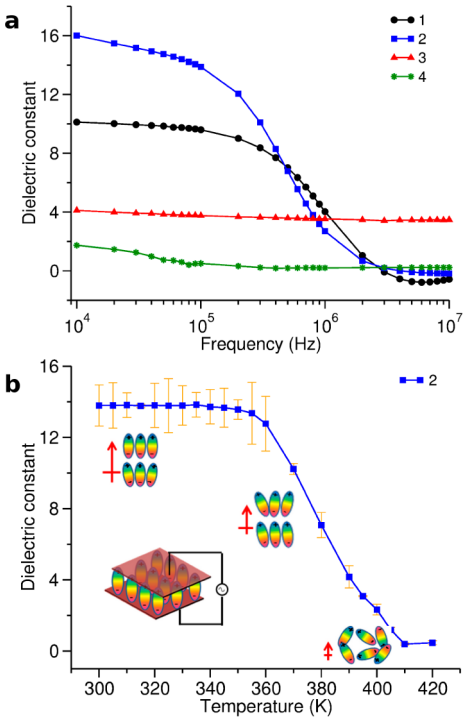

Figure 6. Bulk dielectric measurements. (a) ε_r measurement as a function of frequency. (b) ε_r variation with temperature for molecule **2** at 10 kHz. Inset in (b) shows a schematic of the device and the dipole alignment at different temperatures. The oval-shaped dipoles represent the polarization of an aggregate and not that of individual molecules.

The relaxation dynamics involved in the dipole or an assembly of dipoles is probed by looking into the variation of ε_r as a function of frequency. A decrease in ε_r magnitude at high frequency is observed for molecules **1** and **2**, whereas molecules **3** and **4** demonstrated a flat frequency response (Figure 6a). This response can be directly correlated to the long-range interaction which drives the cooperative assembly. Due to the existence of long-range interaction, the dipoles behave as clusters or domains which have a relatively slower response compared to individual dipoles.[75] Thus, frequency-dependent dielectric studies confirm the presence of significant clustering of dipoles in condensed phase of **1** and **2** and a lack of such interactions for **3** and **4**.

The temperature dependence of dielectric constant reveals the significance of dipole−dipole interaction necessary to drive the cooperative behavior. The ε_r versus temperature curves for molecules **1** (SI, Figure S45a) and **2** (Figure 6b) indicate a

DOI: 10.1021/jacs.5b00504
J. Am. Chem. Soc. XXXX, XXX, XXX−XXX

critical temperature where the ε_r starts to decrease, and for higher temperatures (390−420 K) ε_r = 1−2 is obtained. This behavior can be correlated to the cooperative nature of the individual molecular dipoles which result in a macroscopic polarization. As the temperature increases, the thermal-disorder decreases the dipole−dipole interaction between monomers in an assembly. It is to be noted here that the assembly is not completely disassembled at higher temperatures (see SI, Figure S46); rather, the dipole−dipole interactions have vanished. It is also observed that $\omega_{bandwidth}$ (where ε_r decreases by a factor of 2) has a monotonous dependence with temperature; i.e., a slower relaxation at low temperature indicates a larger range of interaction and coupling of the dipoles in form of clusters, while the upper limit of relaxation is achieved at high T and corresponds to the classical independent dipole ($\varepsilon_{classical\text{-}dipole}$) relaxation limit (see SI, Figure S47b). These findings suggest that temperature-dependent ε_r measurements can be used as an electrical probe for monitoring the presence of dipole−dipole interactions, which are critical in governing the mechanism of self-assembly. In the case of molecules **3** and **4**, which exhibit isodesmic mechanism, a typical Arrhenius behavior is observed for $\varepsilon_r(T)$ (see SI, Figure S45b,c). Thus, cooperativity or otherwise in the assembly mechanism can also be observed using dielectric measurements.

DISCUSSION

The different mechanisms of self-assembly observed in the present systems can be rationalized at a molecular level, based on MD simulation and bulk dielectric measurements as summarized below. For molecules **1** and **2**, the carbonate linkers are closely packed in an ordered manner leading to an enhanced interaction between them, which is reflected in the magnitude of its macro-dipole moment and dielectric constant. Between **1** and **2**, the latter shows higher cooperativity, more negative free energy of polymerization, and higher dielectric constant. This could be mainly due to the planar and rigid conformation of dihydrocholesterol leading to stronger carbonate−carbonate interaction in the assembly compared to molecule **1**. In the case of **3**, although the assembly is ordered, it does not lead to a high macro-dipole moment since the dipole moment of ether linkers is small; no appreciable long-range interaction is possible, and the molecule assembles in an isodesmic manner. Similarly, although **4** possesses dipolar carbonate groups, because of the lack of ordered organization wrought by the flexibility of chiral swallowtails, no macro-dipole moment is observed, resulting in its isodesmic polymerization. Cooperative self-assembly is observed for **PBI_carb_dd** containing dodecycl chains as the self-assembling moiety and carbonate groups as linkers; this again suggests that the linear dodecyl chain can pack better through van der Waals interactions, leading to strengthening of the carbonate−carbonate interaction. Thus, the rigidity/flexibility of the self-assembling moiety reinforces the dipolar interactions between the monomers in the assembly.

CONCLUSION

We have studied the mechanism of self-assembly of four PBI derivatives appended with different linkers and self-assembling moieties, in an attempt to elucidate the molecular features governing the mechanism of supramolecular polymerization. For molecules following a cooperative mechanism of self-assembly (**1** and **2**), significant macro-dipole or polarization was observed through both MD simulation and bulk dielectric measurements. However, the absence of either the dipolar carbonate group, as in molecule **3**, or a suitable self-assembling moiety, as in molecule **4**, results in an isodesmic self-assembly without any significant polarization for the assembly. Thus, with the aid of careful molecular design, MD simulation, and bulk dielectric measurements, we are able to provide a proof-of-concept example for the long-range interaction-driven cooperative self-assembly, as hypothesized earlier.[35] It is also to be noted that polarization or macro-dipole only in the stacking direction is critical in governing the mechanism of self-assembly. Presently studies are underway in our laboratory to apply the same concepts to other π-conjugated molecules and to look at the generality of the above conclusions.

ASSOCIATED CONTENT

Supporting Information

Synthesis and characterization details for **1**−**4**; computational and dielectric measurement details; supporting figures and tables. This material is available free of charge via the Internet at http://pubs.acs.org.

AUTHOR INFORMATION

Corresponding Authors

*bala@jncasr.ac.in

*george@jncasr.ac.in

Notes

The authors declare no competing financial interest.

ACKNOWLEDGMENTS

The authors thank Department of Science and Technology (DST), India, for financial support. S.J.G. and S.B. gratefully acknowledge Sheikh Saqr Career Award. C.K. thanks Prof. A. J. Markvoort and Prof. ten H. M. M. Eikelder from TU/e for suggestions on modeling experimental data, and Mr. V. K. Bharadwaj for aid in synthesis of molecule **1**. C. K. acknowledges Mr. Kumaraswamya from Malvern for DLS, and Mr. Hitesh Khandelwal and Ralf Bovee from TU/e for MALDI-TOF measurements. The authors also thank Prof. E. W. Meijer for comments on the manuscript.

REFERENCES

(1) Hoeben, F. J. M.; Jonkheijm, P.; Meijer, E. W.; Schenning, A. P. H. J. *Chem. Rev.* **2005**, *105*, 1491.
(2) Brunsveld, L.; Folmer, B. J. B.; Meijer, E. W.; Sijbesma, R. P. *Chem. Rev.* **2001**, *101*, 4071.
(3) Babu, S. S.; Praveen, V. K.; Ajayaghosh, A. *Chem. Rev.* **2014**, *114*, 1973.
(4) Aida, T.; Meijer, E. W.; Stupp, S. I. *Science* **2012**, *335*, 813.
(5) Stupp, S. I.; Palmer, L. C. *Chem. Mater.* **2013**, *26*, 507.
(6) Zelzer, M.; Ulijn, R. V. *Chem. Soc. Rev.* **2010**, *39*, 3351.
(7) Faramarzi, V.; Niess, F.; Moulin, E.; Maaloum, M.; Dayen, J.-F.; Beaufrand, J.-B.; Zanettini, S.; Doudin, B.; Giuseppone, N. *Nat. Chem.* **2012**, *4*, 485.
(8) Ogi, S.; Sugiyasu, K.; Manna, S.; Samitsu, S.; Takeuchi, M. *Nat. Chem.* **2014**, *6*, 188.
(9) Gilroy, J. B.; Gädt, T.; Whittell, G. R.; Chabanne, L.; Mitchels, J. M.; Richardson, R. M.; Winnik, M. A.; Manners, I. *Nat. Chem.* **2010**, *2*, 566.
(10) Hudson, Z. M.; Lunn, D. J.; Winnik, M. A.; Manners, I. *Nat. Commun.* **2014**, *5*, No. 3372.
(11) Kang, J.; Miyajima, D.; Mori, T.; Inoue, Y.; Itoh, Y.; Aida, T. *Science* **2015**, *347*, 646.

DOI: 10.1021/jacs.5b00504
J. Am. Chem. Soc. XXXX, XXX, XXX−XXX

(12) Ogi, S.; Fukui, T.; Jue, M. L.; Takeuchi, M.; Sugiyasu, K. *Angew. Chem., Int. Ed.* **2014**, *53*, 14363.
(13) Jain, A.; George, S. J. *Mater. Today* **2015**, DOI: 10.1016/j.mattod.2015.01.015.
(14) De Greef, T. F. A.; Smulders, M. M. J.; Wolffs, M.; Schenning, A. P. H. J.; Sijbesma, R. P.; Meijer, E. W. *Chem. Rev.* **2009**, *109*, 5687.
(15) Sept, D.; McCammon, J. A. *Biophys. J.* **2001**, *81*, 667.
(16) Abram, D.; Koffler, H. *J. Mol. Biol.* **1964**, *9*, 168.
(17) Chen, Z.; Lohr, A.; Saha-Möller, C. R.; Würthner, F. *Chem. Soc. Rev.* **2009**, *38*, 564.
(18) Zhao, D.; Moore, J. S. *Org. Biomol. Chem.* **2003**, *1*, 3471.
(19) Smulders, M. M. J.; Schenning, A. P. H. J.; Meijer, E. W. *J. Am. Chem. Soc.* **2008**, *130*, 606.
(20) Cantekin, S.; Balkenende, D. W. R.; Smulders, M. M. J.; Palmans, A. R. A.; Meijer, E. W. *Nat. Chem.* **2011**, *3*, 42.
(21) Smulders, M. M. J.; Nieuwenhuizen, M. M. L.; Grossman, M.; Filot, I. A. W.; Lee, C. C.; de Greef, T. F. A.; Schenning, A. P. H. J.; Palmans, A. R. A.; Meijer, E. W. *Macromolecules* **2011**, *44*, 6581.
(22) Wang, F.; Gillissen, M. A. J.; Stals, P. J. M.; Palmans, A. R. A.; Meijer, E. W. *Chem.—Eur. J.* **2012**, *18*, 11761.
(23) García, F.; Viruela, P. M.; Matesanz, E.; Ortí, E.; Sánchez, L. *Chem.—Eur. J.* **2011**, *17*, 7755.
(24) Helmich, F.; Lee, C. C.; Nieuwenhuizen, M. M. L.; Gielen, J. C.; Christianen, P. C. M.; Larsen, A.; Fytas, G.; Leclère, P. E. L. G.; Schenning, A. P. H. J.; Meijer, E. W. *Angew. Chem., Int. Ed.* **2010**, *49*, 3939.
(25) García, F.; Sánchez, L. *J. Am. Chem. Soc.* **2012**, *134*, 734.
(26) Mayerhöffer, U.; Würthner, F. *Chem. Sci.* **2012**, *3*, 1215.
(27) Aparicio, F.; Matesanz, E.; Sanchez, L. *Chem. Commun.* **2012**, *48*, 5757.
(28) Fenske, M. T.; Meyer-Zaika, W.; Korth, H.-G.; Vieker, H.; Turchanin, A.; Schmuck, C. *J. Am. Chem. Soc.* **2013**, *135*, 8342.
(29) Jonkheijm, P.; van der Schoot, P.; Schenning, A. P. H. J.; Meijer, E. W. *Science* **2006**, *313*, 80.
(30) Tomović, Ž.; van Dongen, J.; George, S. J.; Xu, H.; Pisula, W.; Leclère, P.; Smulders, M. M. J.; De Feyter, S.; Meijer, E. W.; Schenning, A. P. H. J. *J. Am. Chem. Soc.* **2007**, *129*, 16190.
(31) Mayoral, M. J.; Rest, C.; Stepanenko, V.; Schellheimer, J.; Albuquerque, R. Q.; Fernández, G. *J. Am. Chem. Soc.* **2013**, *135*, 2148.
(32) Krieg, E.; Weissman, H.; Shimoni, E.; Bar On, A.; Rybtchinski, B. *J. Am. Chem. Soc.* **2014**, *136*, 9443.
(33) Rest, C.; Mayoral, M. J.; Fucke, K.; Schellheimer, J.; Stepanenko, V.; Fernández, G. *Angew. Chem., Int. Ed.* **2014**, *53*, 700.
(34) Li, L.; Yuan, C.; Dai, L.; Thayumanavan, S. *Macromolecules* **2014**, *47*, 5869.
(35) Kulkarni, C.; Balasubramanian, S.; George, S. J. *ChemPhysChem* **2013**, *14*, 661.
(36) Würthner, F.; Yao, S.; Beginn, U. *Angew. Chem., Int. Ed.* **2003**, *42*, 3247.
(37) Fernández, G.; Stolte, M.; Stepanenko, V.; Würthner, F. *Chem.—Eur. J.* **2013**, *19*, 206.
(38) Würthner, F.; Stolte, M. *Chem. Commun.* **2011**, *47*, 5109.
(39) Würthner, F. *Chem. Commun.* **2004**, 1564.
(40) Ikeda, T.; Masuda, T.; Hirao, T.; Yuasa, J.; Tsumatori, H.; Kawai, T.; Haino, T. *Chem. Commun.* **2012**, *48*, 6025.
(41) Würthner, F.; Thalacker, C.; Diele, S.; Tschierske, C. *Chem.—Eur. J.* **2001**, *7*, 2245.
(42) Chen, Z.; Stepanenko, V.; Dehm, V.; Prins, P.; Siebbeles, L. D. A.; Seibt, J.; Marquetand, P.; Engel, V.; Würthner, F. *Chem.—Eur. J.* **2007**, *13*, 436.
(43) van Herrikhuyzen, J.; Syamakumari, A.; Schenning, A. P. H. J.; Meijer, E. W. *J. Am. Chem. Soc.* **2004**, *126*, 10021.
(44) Kaiser, T. E.; Stepanenko, V.; Würthner, F. *J. Am. Chem. Soc.* **2009**, *131*, 6719.
(45) van der Weegen, R.; Korevaar, P. A.; Voudouris, P.; Voets, I. K.; de Greef, T. F. A.; Vekemans, J. A. J. M.; Meijer, E. W. *Chem. Commun.* **2013**, *49*, 5532.
(46) Yagai, S.; Usui, M.; Seki, T.; Murayama, H.; Kikkawa, Y.; Uemura, S.; Karatsu, T.; Kitamura, A.; Asano, A.; Seki, S. *J. Am. Chem. Soc.* **2012**, *134*, 7983.
(47) Seki, T.; Asano, A.; Seki, S.; Kikkawa, Y.; Murayama, H.; Karatsu, T.; Kitamura, A.; Yagai, S. *Chem.—Eur. J.* **2011**, *17*, 3598.
(48) Reddy, S. K.; Balasubramanian, S. *J. Phys. Chem. B* **2012**, *116*, 14892.
(49) Chloroformates were either obtained from commercial source or synthesized by the chloroformylation of the corresponding alcohols using triphosgene following the reported procedure. See SI for details.
(50) Adachi, M.; Murata, Y.; Nakamura, S. *J. Phys. Chem.* **1995**, *99*, 14240.
(51) Abraham, S.; Vijayaraghavan, R. K.; Das, S. *Langmuir* **2009**, *25*, 8507.
(52) Svobodova, H.; Noponen, V.; Kolehmainen, E.; Sievanen, E. *RSC Adv.* **2012**, *2*, 4985.
(53) Sugiyasu, K.; Fujita, N.; Shinkai, S. *Angew. Chem., Int. Ed.* **2004**, *43*, 1229.
(54) Murata, K.; Aoki, M.; Suzuki, T.; Harada, T.; Kawabata, H.; Komori, T.; Ohseto, F.; Ueda, K.; Shinkai, S. *J. Am. Chem. Soc.* **1994**, *116*, 6664.
(55) Ajayaghosh, A.; Vijayakumar, C.; Varghese, R.; George, S. J. *Angew. Chem., Int. Ed.* **2006**, *45*, 456.
(56) Although **1** is completely soluble in MCH, the aggregates could not be disassembled with increase in temperature. Thus, to control the extent of self-assembly such that diassembly could be achieved, a fraction of good solvent (TCE) was used.
(57) The data are not shown. Also, a systematic study of the variation of CD spectra as a function of cooling rate and aging is beyond the scope of this work and will be investigated in detail as a separate work.
(58) Lu, L.; Cocker, T. M.; Bachman, R. E.; Weiss, R. G. *Langmuir* **2000**, *16*, 20.
(59) Smulders, M. M. J.; Nieuwenhuizen, M. M. L.; de Greef, T. F. A.; van der Schoot, P.; Schenning, A. P. H. J.; Meijer, E. W. *Chem.—Eur. J.* **2010**, *16*, 362.
(60) ten Eikelder, H. M. M.; Markvoort, A. J.; de Greef, T. F. A.; Hilbers, P. A. J. *J. Phys. Chem. B* **2012**, *116*, 5291.
(61) Markvoort, A. J.; ten Eikelder, H. M. M.; Hilbers, P. A. J.; de Greef, T. F. A.; Meijer, E. W. *Nat. Commun.* **2011**, *2*, 509.
(62) Huang, X.; Raghavan, S. R.; Terech, P.; Weiss, R. G. *J. Am. Chem. Soc.* **2006**, *128*, 15341.
(63) Because of the low solubility and the presence of multiple stereocenters in **3**, reliable CD spectra (under thermodynamic control) could not be achieved; thus, temperature-dependent UV/vis studies were performed.
(64) The isodesmic fits to the cooling curves for **3** and **4** show slight deviations from the experimental data. Since these cooling curves are obtained from UV/vis studies, the deviation could be due to the small change in absorbance at the monitored wavelength. The fit is sub-isodesmic in the case of **3**; thus, this molecule can be weakly cooperative, which adds further to the deviation from the fit.
(65) Brocorens, P.; Linares, M.; Guyard-Duhayon, C.; Guillot, R.; Andrioletti, B.; Suhr, D.; Isare, B.; Lazzaroni, R.; Bouteiller, L. *J. Phys. Chem. B* **2013**, *117*, 5379.
(66) Bejagam, K. K.; Fiorin, G.; Klein, M. L.; Balasubramanian, S. *J. Phys. Chem. B* **2014**, *118*, 5218.
(67) Danila, I.; Riobé, F.; Piron, F.; Puigmartí-Luis, J.; Wallis, J. D.; Linares, M.; Ågren, H.; Beljonne, D.; Amabilino, D. B.; Avarvari, N. *J. Am. Chem. Soc.* **2011**, *133*, 8344.
(68) Marty, R.; Nigon, R.; Leite, D.; Frauenrath, H. *J. Am. Chem. Soc.* **2014**, *136*, 3919.
(69) Roche, C.; Sun, H.-J.; Prendergast, M. E.; Leowanawat, P.; Partridge, B. E.; Heiney, P. A.; Araoka, F.; Graf, R.; Spiess, H. W.; Zeng, X.; Ungar, G.; Percec, V. *J. Am. Chem. Soc.* **2014**, *136*, 7169.
(70) Klein, M. L.; Shinoda, W. *Science* **2008**, *321*, 798.
(71) MD simulations were not performed for **2** because of its structural similarity to molecule **1**.
(72) Senanayak, S. P.; Guha, S.; Narayan, K. S. *Phys. Rev. B* **2012**, *85*, 115311.

DOI: 10.1021/jacs.5b00504
J. Am. Chem. Soc. XXXX, XXX, XXX−XXX

(73) Ashcroft, N. W.; Mermin, N. D. *Solid state physics*; Holt, Rinehart and Winston: New York, 1976.
(74) The average dipole moment per molecule obtained from bulk dielectric measurements for molecules **1**, **3**, and **4** is 3.4, 0.7, and 0.5 D, respectively (see SI for details of calculation). The macro-dipole moment obtained from MD simulation was divided by 40 (oligomer size) to obtain the dipole moment per molecule; dipole moments from simulations for **1**, **3**, and **4** are 0.36, 0.05, and 0.03 D, respectively.
(75) Senanayak, S. P.; Narayan, K. S. *Adv. Funct. Mater.* **2014**, *24*, 3324.

DOI: 10.1021/jacs.5b00504
J. Am. Chem. Soc. XXXX, XXX, XXX−XXX